

MODIFICATION OF SOLAR ACTIVITY INDICES IN THE INTERNATIONAL REFERENCE IONOSPHERE IRI AND IRI-Plas MODELS DUE TO RECENT REVISION OF SUNSPOT NUMBER TIME SERIES

T.L. Gulyaeva

*Institute of Terrestrial Magnetism, Ionosphere and Radio Wave Propagation RAS, Moscow, Russia,
gulyaeva@izmiran.ru*

The International Reference Ionosphere (IRI) imports global effective ionospheric IG_{12} index based on ionosonde measurements of the critical frequency f_oF2 as a proxy of solar activity. Similarly, the global electron content (GEC), smoothed by the sliding 12-months window (GEC_{12}), is used as a solar proxy in the ionospheric and plasmaspheric model IRI-Plas. GEC has been calculated from global ionospheric maps of total electron content (TEC) since 1998 whereas its productions for the preceding years and predictions for the future are made with the empirical model of the linear dependence of GEC on solar activity. At present there is a need to re-evaluate solar and ionospheric indices in the ionospheric models due to the recent revision of sunspot number (SSN2) time series, which has been conducted since July 1, 2015 [Clette et al., 2014]. Implementation of SSN2 instead of the former SSN1 series with the ionospheric model could increase model prediction errors. A formula is proposed to transform the smoothed SSN2₁₂ series to the proxy of the former basic SSN1₁₂= R_{12} index, which is used by the IRI and IRI-Plas models for long-term ionospheric predictions. Regression relationships are established between GEC_{12} , the sunspot number R_{12} , and the proxy solar index of 10.7 cm microwave radio flux, $F10.7_{12}$. Comparison of calculations by the IRI-Plas and IRI models with observations and predictions for Moscow during solar cycles 23 and 24 has shown the advantage of implementation of GEC_{12} index with the IRI-Plas model.

Keywords Global electron content · Sunspot number · Solar radio flux · Ionosphere · Plasmasphere · Models IRI, IRI-Plas

INTRODUCTION

Transionospheric radio wave propagation provides conditions for signal transmission in Earth-to-space and satellite-to-satellite communications. To ensure reliability of signal transmission and reception in long-term space experiments, ionospheric conditions are predicted using well-known models such as the International Reference Ionosphere (IRI), the ionospheric and plasmaspheric model IRI-Plas [Bilitza et al., 2011; Gulyaeva, Bilitza, 2012], the Russian standard model of the ionosphere SMI [Chasovitin et al., 1987], and the empirical model for calculating transionospheric radio wave propagation NeQuick [Nava et al., 2008]. Calculation results depend on what solar and ionospheric control parameters we set in the models. A need has arisen to re-evaluate solar and ionospheric control parameters of the ionospheric models due

to the recent revision of the long-term sunspot number time series over the period from 1818 to the present day [Clette et al., 2014]. The modified sunspot number time series *SSN2* significantly differs from the original long-term series *SSN1*. Values of *SSN2* near the solar maximum are generally higher than those of the proxy solar index of 10.7 cm microwave radio flux, *F10.7*, which, in turn, are on average by 60 units higher than values of *SSN1* [Ahluwalia, 2016]. The direct use of *SSN2* instead of *SSN1* for applied problems, specifically for predictions with the ionospheric models, can cause noticeable model calculation errors.

Some blocks of the ionospheric models IRI, IRI-Plas, SMI, and NeQuick are based on different solar activity indices or their ionospheric equivalents. In these models, 3D representation of electron density relies on fitting of vertical distribution of electron density to the maximum electron density and height of the F2 layer from planetary maps designed by the International Telecommunication Union ITU-R [CCIR Atlas, 1983]. The planetary maps of the critical frequency f_oF2 and radio wave propagation factor M3000F2 related to the height of maximum ionization h_mF2 are derived using the expansion coefficients of the spherical harmonic analysis of these parameters from ionosonde measurements. These coefficients are obtained as a function of latitude, longitude, universal time (UT) from 0 to 24 hr with a step of 1 hr, seasonal variations for twelve months and four solar activity levels $R_{12}=0, 50, 100, 150$, with respective interpolation for intermediate values of these parameters [Jones, Gallett, 1965].

Procedure of IRI calculations of the F2-layer critical frequency f_oF2 (or its related maximum electron density N_mF2) with ITU-R maps uses the effective ionospheric index IG_{12} , derived from f_oF2 measurements by an ionosonde network, as a proxy of solar activity [Liu et al., 1983]. When calculating h_mF2 in the IRI and IRI-Plas models from M3000F2 (ITU-R) maps, the f_oF2 and f_oE and the 12-month smoothed R_{12} , based on the former sunspot number time series *SSN1*, are used [Bilitza et al., 1979]. The ionospheric solar activity index IG [Liu et al., 1983] and the set smoothed by the sliding 12-months window, IG_{12} , are based on noon values of f_oF2 from measurements of 13 ionosondes, scaled to the sunspot numbers R_{12} . The comparison of IG_{12} with R_{12} over the past six solar cycles [Bilitza et al., 2012] shows their differences most pronounced at solar maximum and minimum.

In literature, there are different proxies of solar activity indices used in the ionospheric models. The F_{12} is shown to be more effective than R_{12} for the long-term f_oF2 predictions [Deminov, 2016]. According to [Ratovsky et al., 2015], the local model of F2-layer peak parameters depends linearly on *F10.7*, normalized to $F10.7=100$ i.u. (index unit 1 i.u. = 10^{-22} W·m⁻²·Hz⁻¹). For modeling of total electron content (TEC) maps, the best accuracy is obtained with the proxy index of solar radio flux *F10.7* and sunspot number time series *SSN1* averaged over the sum of three components: 3-day smoothed daily, 7- and 27-day backward mean values [Maruyama, 2010]. The regression relationship between *SSN1* and *F10.7* used by the IRI and IRI-Plas models is valid until 2000, but it is changed after 2001 [Lukianova, Mursula, 2011]. At present, all former estimates of the efficiency of the sunspot number *SSN1* series need revising because this index is not measured any longer since July 1, 2015; instead, solar activity is monitored using the *SSN2* index [Clette et al., 2014].

The f_oF2 and h_mF2 are calculated from ITU-R maps by the IRI-Plas model, using the global electron content of Earth's ionosphere and plasmasphere (*GEC*) produced from TEC maps as a proxy of solar activity [Afraimovich, Perevalova, 2006; Afraimovich et al., 2008; Gulyaeva, Veselovsky, 2014]. The advantage of IRI-Plas model over IRI is the plasmasphere model incorporated in vertical electron density and temperature profiles up to 20 200 km

above the Earth surface (the orbit of GPS satellites), whereas IRI allows calculations only to 2000 km in the ionosphere.

GEC is investigated in the present paper as a proxy of solar activity and compared with other solar and ionospheric indices, taking into account the recent revision of sunspot number time series. The purpose of this study is to update the set of control parameters in the IRI-Plas model, specifically for calculations of maximum electron density and F2-layer height from the source maps, and to warn users of the models against possible errors arising from the modified sunspot number time series implementation with the ionospheric models.

DYNAMICS OF SOLAR AND IONOSPHERIC INDICES

Figure 1 presents dynamics of the 12-month smoothed sunspot number time series $SSN1_{12}$ and $SSN2_{12}$ since 1931, including the prediction for solar cycle 24 until 2019, and of solar radio flux $F10.7_{12}$ since 1957. Values of $F10.7_{12}$ exceed by 40–60 units the corresponding values of $SSN1_{12}$ (Figure 1), and $F10.7_{12}$ has significantly exceeded $SSN2_{12}$ since 2001 [Lukianova, Mursula, 2011]. The new sunspot number time series $SSN2_{12}$ are much higher than $SSN1_{12}$; near maxima of solar cycles 19 and 21 values of $SSN2_{12}$ exceed even $F10.7_{12}$ ones. This has never been observed for $SSN1_{12}$.

The time series $SSN1_{12}$ smoothed by the sliding 12-month window (denoted by R_{12}) are used to scale the control parameters IG_{12} and GEC_{12} for ITU-R calculations and their implementation in the above 3D ionospheric models. The upper limit $R_{12}=150$ restricts the ITU-R set of coefficients due to saturation of the peak electron density in the ionosphere, i.e. the electron density reaches the saturation level and stops increasing with further increasing solar activity [Deminov, 2016]. The saturation effect is illustrated in Figure 2 with IG_{12} calculated from f_0F2 observations [Liu et al., 1983] and plotted against the solar activity index R_{12} . This dependence can be expressed by the second-order polynomial (the solid curve in Figure 2):

$$IG_{12} = -0.0031R_{12}^2 + 1.5332R_{12} - 11.5634. \quad (1)$$

In view of the saturation effect, when the sunspot number R_{12} exceeds 150 units, it is replaced by the limiting value $R_{12}=150$ and the relevant upper limit of the ITU-R set of coefficients is used to calculate parameters of the F2-layer peak, i.e., the ITU-R extrapolation above the saturation limit is not provided. As is shown in Figure 1 and below,

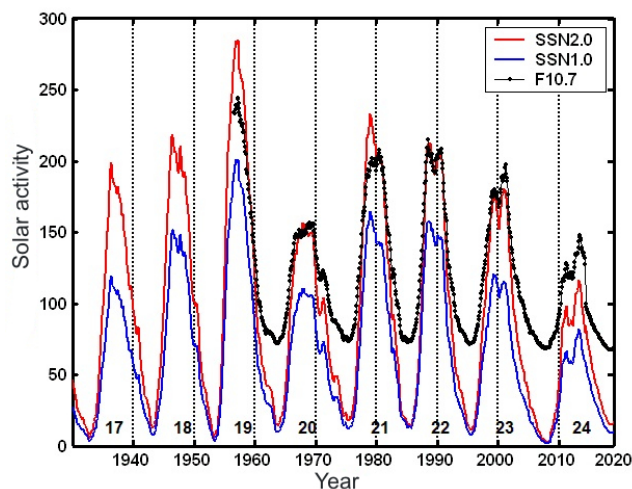


Figure 1. Dynamics of $SSN1_{12}$, $SSN2_{12}$, and $F10.7_{12}$

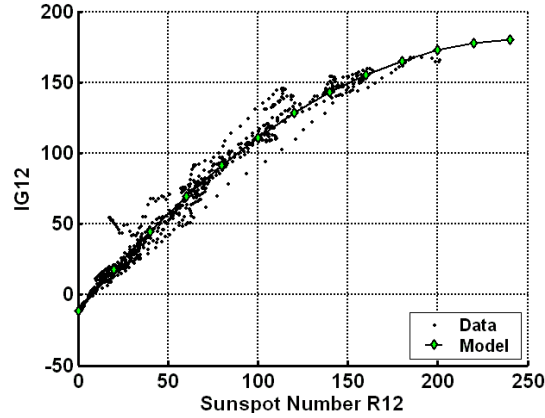


Figure 2. Variation of the ionospheric index IG_{12} calculated from the noon ionosonde network measurements of f_oF_2 in 1957–2015 as a function of R_{12} . The solid curve is the model by formula (1)

such limits are applicable only for the maximum of solar cycle 19 (1957–1958) and partially for the maximum of solar cycle 21 (1980) with SSN_{12} . At the same time, the direct implementation of $SSN_{2,12}$ in calculations with ITU-R maps leads to neglect of the actual values of $SSN_{2,12}$ above the upper saturation limit ($R_{12}=150$) in six solar cycles (17, 18, 19, 21, 22, 23) (Figure 1).

Regression relationships (2) of the primary and new sunspot number time series with the solar radio flux $F_{10.7,12}$ are plotted in Figure 3.

$$Y=AX+B. \tag{2}$$

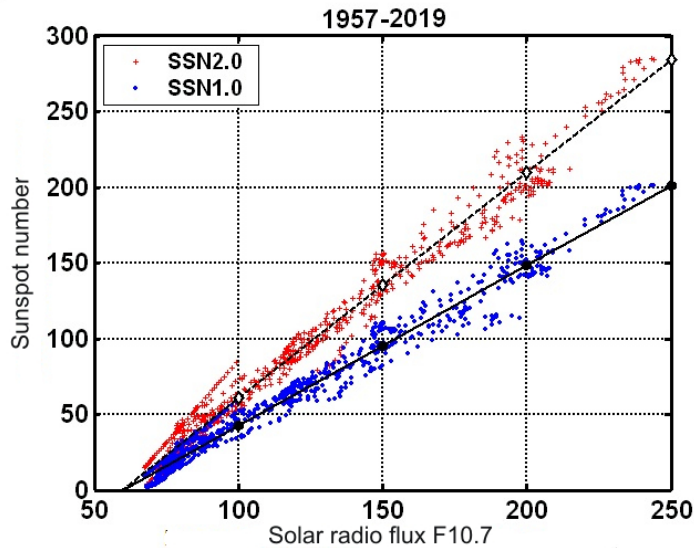


Figure 3. Regression relationship of the old and new sunspot number time series, smoothed by the sliding 12-month window, with the 12-monthly smoothed 10.7 cm (2800 MHz) solar radio flux $F_{10.7,12}$

The parameters X and Y and the coefficients A and B of regression equation (2) are set out in Table 1. Further, regression equation (2) is denoted by the number given in the first column of Table 1, specifying coefficients in the respective lines numbered (2.1), (2.2), etc.

Table 1

Regression coefficients between solar indices smoothed by the sliding 12-months window

№	Y	X	A	B
2.1	$SSN1_{12}$	$F10.7_{12}$	1.0588	-63.2760
2.2	$SSN2_{12}$	$F10.7_{12}$	1.4929	-88.5781
2.3	GEC_{12}	GEC_{12U}	57.5362	-46.0550
2.4	GEC_{12}	$SSN1_{12}$	0.9703	1.4447
2.5	GEC_{12}	$SSN2_{12}$	0.6511	1.1512
2.6	GEC_{12}	$F10.7_{12}$	0.9516	-59.5356

In the absence of observations of $SSN1_{12}$ and $SSN2_{12}$, relevant values could be calculated from their linear dependence on the parameter $F10.7_{12}$ by formulae (2.1) and (2.2). These equations can also be used to resolve ambiguities when it is not clear to which time series – $SSN1_{12}$ or $SSN2_{12}$ – solar datasets belong. Values calculated by formulae (2.1) and (2.2) show to which index set the data pertain.

The most promising is the transformation of $SSN2_{12}$ to the scale of $SSN1_{12}$ in order to obtain model driving parameters for the ITU-R maps, which are based on $SSN1_{12}$. Figure 4 illustrates the linear relationship between $SSN1_{12}$ and $SSN2_{12}$. This relationship suggests that the sunspot number time series $SSN2_{12}$, smoothed by the 12-month window, is brought to the corresponding smoothed series R_{12} ($SSN1_{12}$) with the scaling factor 0.7:

$$R_{12}=0.7SSN2_{12}. \tag{3}$$

Note that this relationship is valid only for the above-mentioned series, smoothed by the sliding 12-month window. Thus, the current $SSN2_{12}$ data unambiguously yield R_{12} , used to guide calculations in the ionospheric models.

The ionospheric GEC parameter representing the integral sum of electrons in near-Earth space at heights from 65 to 20 200 km is measured in units of $GECU=10^{32}$ electrons [Afraimovich, Perevalova, 2006] and varies from 0.1 to 5.0 GECU. Calculations with global TEC maps provide hourly GEC values for 0, 1, ..., 23 UT from observations of GPS satellite signals from September 1998 to the present day. The hourly GEC data are used to derive daily, monthly, 12-month, and other smoothed series of this parameter, which vary within the same limits.

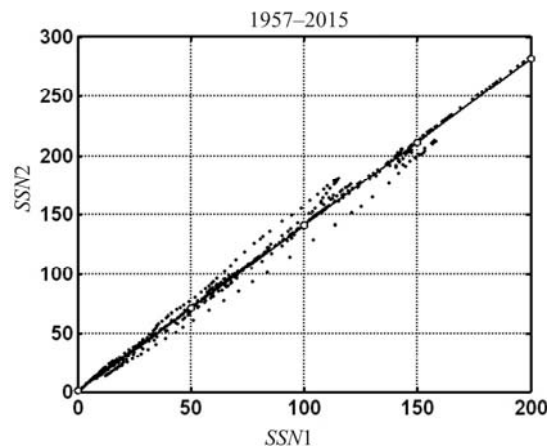


Figure 4. Linear relationship between $SSN1_{12}$ and $SSN2_{12}$

After smoothing the resulting series of monthly GEC values (in GECU) by the sliding 12-month window (designated as the smoothed series by GEC_{12U}) to be used as a proxy of solar activity in IRI-Plas, the GEC_{12U} series is brought to the scale of R_{12} metrics by application of regression equation (2.3) with coefficients set out in line 2.3 of Table 1.

Equation (2.3) is applied to all GEC_{12U} values for the available source global GIM-TEC maps over the period from September 1998 to the present day. To use GEC index series as a proxy of solar activity in the IRI-Plas model, it should be supplemented with the model-reconstructed set of values for the preceding years [Gulyaeva, Veselovsky, 2014].

The GEC_{12U} set of values is permanently updated as new TEC maps become available, hence the model set of coefficients GEC_{12} should be renewed every month. The same is done for the sets of solar activity indices and their prediction for the forthcoming months and years. To regularly update driving parameters of the IRI-Plas model, regression relationships (2.4), (2.5), (2.6) between GEC_{12} and solar activity indices are used. Derivation of these relationships is illustrated in Figure 5, where the regression relationships of GEC_{12} with sunspot number time series SSN_{12} (2.4), SSN_{212} (2.5), and solar radio flux $F_{10.7_{12}}$ (2.6) are plotted. The correlation coefficient between these 12-month smoothed series is 0.9938 (2.4), 0.9955 (2.5), and 0.9962 (2.6) respectively. These equations provide prediction for GEC_{12} , based on the prediction for SSN_{12} (2.4) or $F_{10.7_{12}}$ (2.6) for forthcoming months until December 2019.

Figure 6 illustrates a high accuracy in approximating R_{12} for solar cycles 19–24 by GEC_{12} parameter represented by results of scaling GEC with formula (2.3) from March 1999 to December 2015 and by prediction with formula (2.4) for the rest of years. The equivalent sunspot number R_{F12} calculated from the equation of quadratic regression between F_{12} and R_{12} (see formula (2) [Deminov, 2016]), used by the IRI model [Bilitza, 2015], is also plotted in this figure. It was concluded in [Deminov, 2016] that R_{F12} is more effective than R_{12} for the long-term prediction of f_oF_2 . However, the prediction of f_oF_2 was estimated from the IG_{12} parameter, which differs considerably from R_{12} [Bilitza et al., 2012]. Figure 6 indicates that R_{F12} differs both from R_{12} and GEC_{12} . This difference is greatest near the maxima of solar cycles 21–24. Since ITU-R maps are designed for fixed levels of R_{12} , this particular index and its ionospheric proxy index GEC_{12} are used as model driving parameters of solar activity in the IRI-Plas model.

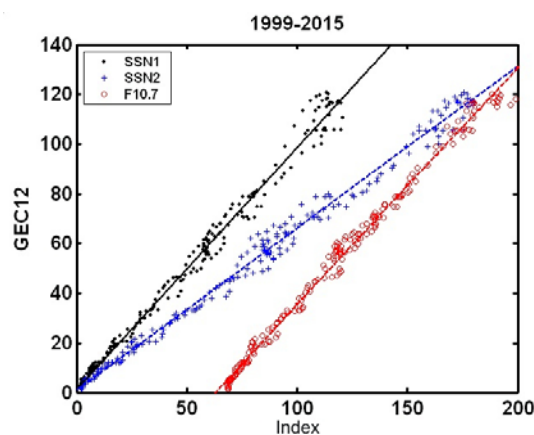


Figure 5. Variation of GEC_{12} with solar activity presented by SSN_{12} , SSN_{212} , and $F_{10.7_{12}}$

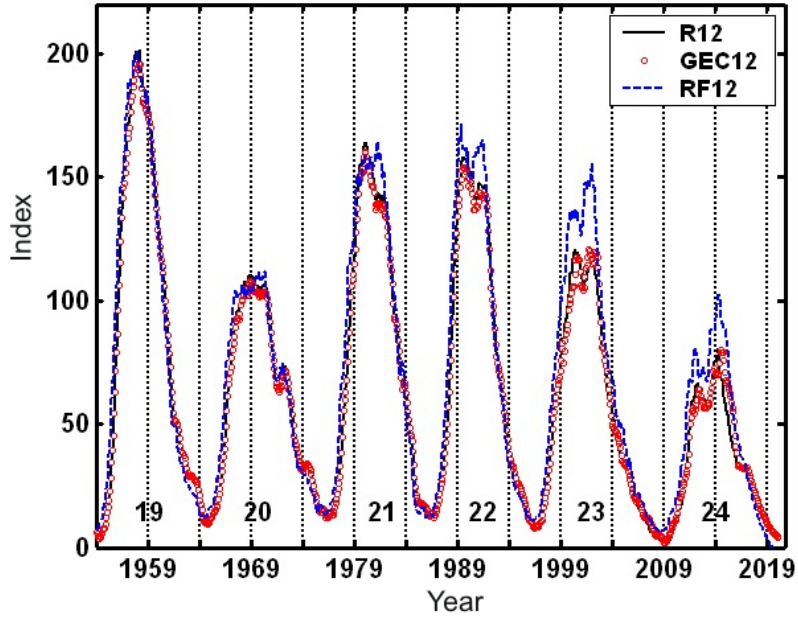


Figure 6. The basic sunspot number index R_{12} in cycles 19–24 and the equivalent solar activity proxy — the global electron content GEC_{12} computed from GIM-TEC maps, scaled to the sunspot number by formula (2.3) from March 1999 to December 2015, and reconstructed by model (2.4) for the rest of years. Model RF_{12} index obtained by reversion of R_{12} to $F10.7_{12}$ index

COMPARING IONOSPHERIC DATA WITH MODEL PREDICTIONS

Variations in SSN_{12} , $SSN_{2,12}$, GEC_{12} , and IG_{12} during solar cycles 19–24 are plotted in Figure 7. The saturation level $R_{12}=150$ for the peak electron density N_mF_2 (proportional to $f_oF_2^2$) is indicated by a horizontal line. In calculating f_oF_2 from ITU-R maps, all values of the above-mentioned indices exceeding 150 units are replaced by this upper limit. Figure 7 clearly shows the part of values that are excluded from calculations in the ionospheric models near solar activity maxima; the greatest losses occur if the $SSN_{2,12}$ is used.

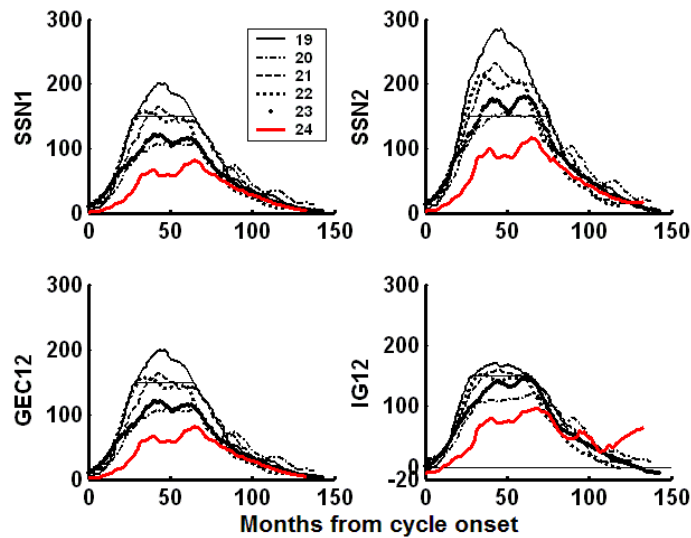


Figure 7. Variations in SSN_{12} , $SSN_{2,12}$, GEC_{12} , and IG_{12} for six solar cycles (19–24)

In this figure, we can see the minimum amplitude of solar cycle 24 with smallest values of all the indices near the solar maximum. The long-term predictions of solar activity refer to the descending phase of solar cycle 24 for 2016–2019. During this period, the IG_{12} index shows appreciable differences with other indices – it increases in 2018–2019 according to data file `ig_rz.dat` of March 10, 2016 in the IRI system [<http://irimodel.org/indices/>].

The prediction for IG_{12} in this period suggests that the minimum of solar cycle 24 is expected on October, 2017. It may happen that the prediction of $SSN1$, $SSN2$, and $F10.7$ for the descending phase of solar activity with the minimum of solar cycle 24 in December 2019 will be corrected as new data become available [Ahluwalia, 2016]. However, differences in the forecast of the driving parameter IG_{12} for the IRI model will result in increased differences of the long-term forecast for model parameters with this index, as is shown below with the said indices used to calculate ionospheric parameters with the IRI and IRI-Plas models for Moscow (55.5° N, 37.3° E).

Figure 8 presents observational data and calculation with the IRI-Plas model for Moscow from 1996 to 2015 in solar cycles 23 and 24. The data on f_oF2 and h_mF2 have been acquired from Parus-A ionosonde observations at IZMIRAN; the TEC data have been calculated from JPL GIM-TEC maps for the above coordinates in Moscow. Calculations by the IRI-Plas model were made with ITU-R maps based on the two solar activity indices $SSN1_{12}$ and $SSN2_{12}$. The comparison between results for solar cycles 23 and 24 shows that the ionospheric ionization was weaker in cycle 24 than in cycle 23, as is also demonstrated by ionosonde observations performed in Japan and by the global-average TEC obtained in [Hao et al., 2014].

The low level of solar extreme ultraviolet emission (EUV) observed during the prolonged solar activity minimum in 2007–2009 still exists in cycle 24, being responsible for the decreased ionospheric plasma ionization. As for calculations with the IRI-Plas model, the ionospheric parameters obtained using $SSN2_{12}$ exceed observed data and values calculated with $SSN1_{12}$. The maximum excess of average monthly values calculated with $SSN2_{12}$ over observed ones is 32 % for f_oF2 , 12 % for h_mF2 , and 38 % for TEC. These differences can vary depending on the time of day, season, geographic and geomagnetic coordinates of an observation point, and on solar activity level.

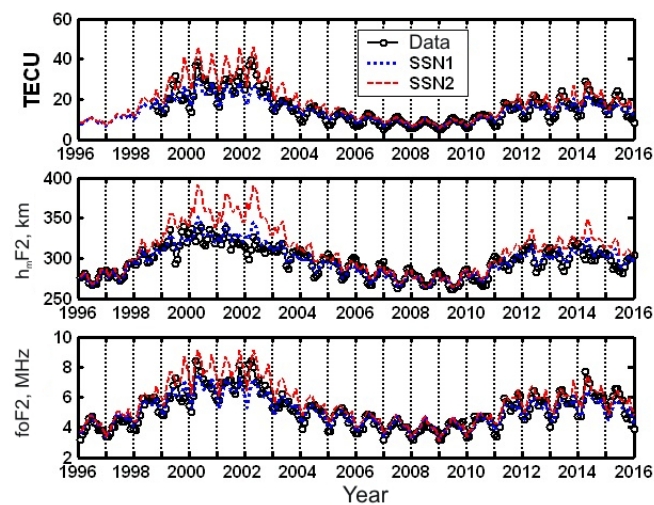


Figure 8. Comparison between observed data and forecast made with the IRI-Plas model ($SSN1$, $SSN2$) for Moscow from 1996 to 2015 in solar cycles 23 and 24. The parameters f_oF2 and h_mF2 as inferred from Parus-A ionosonde observations made at IZMIRAN and TEC data acquired using JPL GIM-TEC maps for Moscow

The current forecast of solar activity indices for 2016–2019 has been employed to predict the ionospheric parameters f_0F2 , h_mF2 , and TEC for Moscow. Although the period of time in this case is beyond the existing ionospheric database so that the model calculation cannot be compared with observations, let us take results of calculation with $R_{12}=SSN_{12}$ as the basic index, on which the ITU-R maps are based, to be the reference level. The results of the prediction produced by the IRI-Plas and IRI models are illustrated in Figure 9. Annual RMS deviations from calculations with the basic solar activity index are listed in Table 2. The results show the best agreement with the baseline forecast (the smallest RMS deviations) using GEC_{12} to predict f_0F2 , h_mF2 , and TEC with the IRI-Plas model.

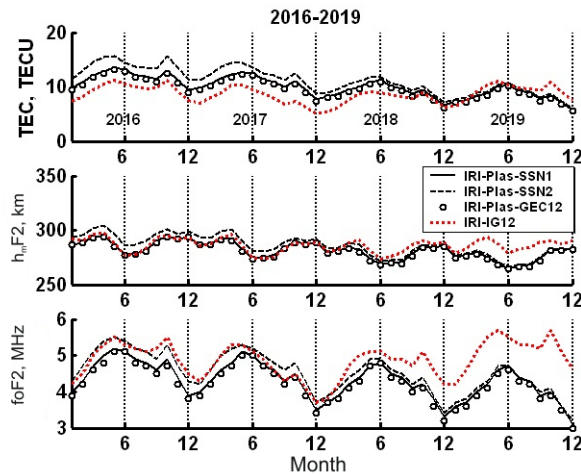


Figure 9. Results of the forecast of f_0F2 , h_mF2 , and TEC for Moscow for 2016–2019 in solar cycle 24 with given solar and ionospheric indices driving the IRI and IRI-Plas models

Table 2

RMS deviation (in measuring units and %) of results of the forecast of ionospheric parameters for Moscow for 2016–2019 guided by the indices SSN_{12} , GEC_{12} , and IG_{12} from the calculation with the basic index $R_{12}=SSN_{12}$ (the average annual value is designated with the brackets)

Year	$\langle f_0F2 \rangle$	RMS		$\langle h_mF2 \rangle$	RMS		$\langle TEC \rangle$	RMS	
	MHz	MHz	%	km	km	%	TECU	TECU	%
IRI-Plas, $SSN_{12} \sim SSN_{12}$									
2016	5.0	0.37	8.0	295.6	7.52	2.6	13.8	2.40	20.3
2017	4.7	0.29	6.4	290.4	6.07	2.1	12.3	1.76	16.3
2018	4.3	0.15	3.6	281.5	3.25	1.2	10.0	0.86	9.3
2019	4.1	0.07	1.8	276.1	1.56	0.6	8.7	0.40	4.9
IRI-Plas, $GEC_{12} \sim SSN_{12}$									
2016	4.5	0.12	2.5	287.5	1.34	0.5	11.4	0.56	4.7
2017	4.4	0.11	2.5	283.9	1.33	0.5	10.4	0.49	4.5
2018	4.1	0.12	2.8	277.5	1.54	0.6	8.9	0.46	5.0
2019	3.9	0.12	2.9	273.7	1.57	0.6	8.0	0.42	5.1
IRI, $IG_{12} \sim SSN_{12}$									
2016	5.0	0.44	9.5	289.9	3.79	1.3	9.6	2.34	19.8
2017	4.6	0.27	6.1	285.1	2.88	1.0	8.0	2.96	27.4
2018	4.7	0.64	15.2	283.9	6.96	2.5	7.8	1.77	19.1
2019	5.2	1.31	32.7	286.4	14.64	5.3	9.3	2.16	26.0

The implementation of the $SSN2_{12}$ index in the IRI-Plas model yields overestimated values the most pronounced in 2016 and decreasing to the minimum of cycle 24. An opposite trend occurs with the IG_{12} index used in the IRI model: predicted parameters overestimate the base calculation results by the end of the period under study.

The TEC results obtained with the IRI model for 2016–2018 underestimate the base calculation output due to integration of TEC in the IRI model only below 2000 km, whereas the base calculation with the IRI-Plas model includes heights up to 20 200 km. However, for 2019 the TEC values predicted by the IRI model exceed those calculated with the base model due to increasing index IG_{12} . One can mitigate the IRI calculation difference with the base index output towards the end of solar cycle 24, using IG_{12} coefficients computed with formula (1) from prediction of sunspots R_{12} for 2016–2019.

Such replacement of IG_{12} can be easily made with formula (1) at online computation on IRI website instead of using default coefficients provided in `ig_rz.dat`.

CONCLUSIONS

In this paper, the solar activity indices used by the IRI-Plas and IRI models are examined. It is shown that the recent modification of the sunspot number time series $SSN2$ [Clette et al., 2014] requires modification and selective implementation of solar and ionospheric model driving parameters. The scaling factor 0.7 is established to convert the new series $SSN2_{12}$ index to basic sunspot number indices $R_{12}=SSN1_{12}$, smoothed by the 12-month window. Regression relationships are introduced between GEC_{12} , R_{12} , and $F10.7_{12}$. The comparison of IRI-Plas calculations with observations at Moscow in solar cycles 23 and 24 demonstrates the advantage of $SSN1_{12}$ over $SSN2_{12}$. The comparison between IRI-Plas and IRI predictions for Moscow for 2016–2019 in the descending phase of cycle 24 shows the least deviation from the forecast made with the original series R_{12} , using GEC_{12} with the IRI-Plas model.

The IRI and IRI-Plas users should be careful specifying parameters of solar activity in these models, namely, by examining the sunspot number time series put online for compliance with the set of basic indices $R_{12}=SSN1_{12}$, which form the basis of ITU-R maps of parameters of the F2-layer maximum. In view of the difference between the forecast of IG_{12} and other solar activity indices, it is advisable to use the index IG_{12} from formula (1) with the IRI model based on the forecast of the sunspot number time series R_{12} for the forthcoming years.

The author thanks SIDC, Belgium, for the $SSN1$ and $SSN2$ indices [<http://sidc.oma.be/silso/>]; SWC, Canada, for data on $F10.7$ [ftp://ftp.geolab.nrcan.gc.ca/data/solar_flux/daily_flux_values/]; IZMIRAN, Moscow, for Parus ionosonde data [<http://www.izmiran.ru/services/iweather/>]; JPL, U.S., for GIM-TEC maps [ftp://sideshow.jpl.nasa.gov/pub/iono_daily/]; D. Bilitza, U.S., for coefficients and online IRI calculations [<http://irimodel.org/indices/>]. The IRI-Plas model is provided by IZMIRAN [<http://ftp.izmiran.ru/pub/izmiran/SPIM/>]. Online IRI-Plas calculations are made on the IONOLAB website [<http://www.ionolab.org/>]. This work is partly supported by grant TUBITAK EEEAG 115E915. The contribution of two reviewers making valuable comments and suggestions is gratefully appreciated.

REFERENCES

- Afraimovich E.L., Perevalova N.P. GPS-Monitoring verkhnej atmosfery Zemli [GPS-Monitoring of the Upper Atmosphere of the Earth]. Irkutsk: ISTP SB RAS, 2006, 480 p. (In Russian).
- Afraimovich E.L., Astafyeva E.I., Oinats A.V., Yasukevich Yu.V., Zhivetiev I.V. Global electron content: a new conception to track solar activity. *Ann. Geophys.* 2008, vol. 26, no. 2, pp. 335–344.
- Ahluwalia H.S. The descent of the solar cycle 24 and future space weather. *Adv. Space Res.* 2016, vol. 57, iss. 2, pp. 710–714. DOI: 10.1016/j.asr.2015.11.015.
- Bilitza D., Sheikh N.M., Eyfrig R. A global model for the height of the F2 peak using M3000 values from the CCIR. *Telecomm. J.* 1979, vol. 46, pp. 549–553.
- Bilitza D., McKinnell L.A., Reinisch B., Fuller-Rowell T. The international reference ionosphere today and in the future. *J. Geodesy.* 2011, vol. 85, pp. 909–920. DOI: 10.1007/s00190-010-0427-x.
- Bilitza D., Brown S.A., Wang M.Y., Souza J.R., Roddy P.A. Measurements and IRI model predictions during the recent solar minimum. *J. Atmos. Solar-Terr. Phys.* 2012, vol. 86, pp. 99–106. DOI: 10.1016/j.jastp.2012.06.010.
- Bilitza D. The International Reference Ionosphere — Status 2013. *Adv. Space Res.* 2015, vol. 55, iss. 8, pp. 1914–1927. DOI: 10.1016/j.asr.2014.07.032.
- CCIR Atlas of Ionospheric Characteristics. *Comite Consultatif International des Radio Communications Rep. 340*. Geneve, International Telecommunication Union, 1983.
- Chasovitin Yu.K., Shirochkov A.V., Besprozvannaya A.S., Gulyaeva T.L., Denisenko P.F., Armenskaya O.A., Ivanova S.E., Kashirin A.I., Klueva N.M., Koryakina E.A., Mironova L.S., Sykilinda T.N., Shushkova V.B., Vodolazkin V.I., Sotsky V.V., Sheidakov N.E. An empirical model for the global distribution of density, temperature and effective collision frequency of electrons in the ionosphere. *Adv. Space Res.* 1987, vol. 7, iss. 6, pp. 49–52.
- Clette F., Svalgaard L., Vaquero J.M., Cliver E.W. Revisiting the sunspot number: a 400-year perspective on the solar cycle. *Space Sci. Rev.* 2014, vol. 186, iss. 1, pp. 35–103.
- Gulyaeva T.L., Bilitza D. Towards ISO Standard Earth Ionosphere and Plasmasphere Model. *New Developments in the Standard Model*. Nova Science Publishers Inc., 2012, pp. 1–39. Available at https://www.novapublishers.com/catalog/product_info.php?products_id=35812 (accessed September 1, 2016).
- Gulyaeva T.L., Veselovsky I.S. Imaging Global Electron Content backwards in time more than 160 years ago. *Adv. Space Res.* 2014, vol. 53, iss. 3, pp. 403–411. DOI: 10.1016/j.asr.2013.11.036.
- Deminov M.G. Solar activity index for long-term ionospheric forecasts. *Cosmic Research.* 2016, vol. 54, no. 1, pp. 1–7. DOI: 10.1134/S0010952516010068.
- Hao Y.Q., Shi H., Xiao Z., Zhang D.H. Weak ionization of the global ionosphere in solar cycle 24. *Ann. Geophys.* 2014, vol. 32, pp. 809–816. DOI: 10.5194/angeo-32-809-2014.
- Jones W.B., Gallet R.M. Representation of diurnal and geographical variations of ionospheric data by numerical method. *Telecomm. J.* 1962, vol. 29, p. 129; 1965, vol. 32, p. 18.
- Liu R., Smith P., King J. A new solar index which leads to improved f_0F_2 prediction using the CCIR atlas. *Telecomm. J.* 1983, vol. 50, pp. 408–414.
- Lukianova R., Mursula K. Changed relation between sunspot numbers, solar UV/EUV radiation and TSI during the declining phase of solar cycle 23. *J. Atmos. Solar-Terr. Phys.* 2011, vol. 73, iss. 2–3, pp. 235–240. DOI: 10.1016/j.jastp.2010.04.002.
- Maruyama T. Solar proxies pertaining to empirical ionospheric total electron content models. *J. Geophys. Res.* 2010, vol. 115, A04306. DOI: 10.1029/2009JA014890.
- Nava B., Coisson P., Radicella S.M. A new version of the NeQuick ionosphere electron density model. *J. Atmosph. Solar-Terr. Phys.* 2008, vol. 70, iss. 15, pp. 1856–1862. DOI: 10.1016/j.jastp.2008.01.015.
- Ratovsky K.G., Oinats A.V., Medvedev A.V. Similarities and differences between regular variations of F2-layer parameters of the polar and midlatitude ionosphere in East Siberian sector. *Solnechno-zemnaya fizika [Solar-Terr. Phys.]*. 2015, vol. 1, no. 2, pp. 70–79. DOI: 10.12737/7832. (In Russian).

URL: <http://sidc.oma.be/silso/> (accessed September 1, 2016).

URL: ftp://ftp.geolab.nrcan.gc.ca/data/solar_flux/daily_flux_values/ (accessed September 1, 2016).

URL: <http://www.izmiran.ru/services/iweather/> (accessed September 1, 2016).

URL: ftp://sideshow.jpl.nasa.gov/pub/iono_daily/ (accessed September 1, 2016).

URL: <http://irimodel.org/indices/> accessed September 1, 2016).

URL: <http://ftp.izmiran.ru/pub/izmiran/SPIM/> (accessed September 1, 2016).

URL: <http://www.ionolab.org/> (accessed September 1, 2016).